Atmos. Chem. Phys., 9, 9249–9261, 2009
www.atmos-chem-phys.net/9/9249/2009/

Atmospheric Chemistry and Physics

Aerosol vertical distribution and optical properties over M'Bour (16.96° W; 14.39° N), Senegal from 2006 to 2008

J.-F. Léon[1,*], Y. Derimian[1], I. Chiapello[1], D. Tanré[1], T. Podvin[1], B. Chatenet[2], A. Diallo[3], and C. Deroo[1]

[1]Laboratoire d'Optique Atmosphérique, CNRS-Université de Lille 1, Villeneuve d'Ascq, France
[2]Laboratoire Inter-Universitaire des systèmes Atmosphériques, CNRS-Université de Paris 7–12, Créteil, France
[3]Institut de Recherche pour le Développement, Dakar, Senegal
[*]now at: Laboratoire d'Aérologie, CNRS-Université Paul Sabatier, Toulouse, France

Received: 16 June 2009 – Published in Atmos. Chem. Phys. Discuss.: 30 July 2009
Revised: 9 November 2009 – Accepted: 25 November 2009 – Published: 8 December 2009

Abstract. We present ground-based measurements of aerosol mass, optical properties and vertical extinction profiles acquired in M'Bour, Senegal (16.96° W; 14.39° N) from January 2006 to September 2008. This place of the world is all year long affected by the export of mineral dust as it moves westward to the north Atlantic ocean. The maximum in the dust activity is observed in summer (June–July), corresponding to a maximum in the aerosol optical thickness (above 0.5) and single scattering albedo (above 0.95). It also corresponds to a maximum in the top altitude of the transported aerosol layer (up to 6 km) and aerosol optical thickness scale height (up to 3.5 km) due to the presence of the Saharan Air Layer located between 2 and 6 km. The late summer shows an additional low level aerosol layer that increases in thickness in autumn. Severe dust storms are also systematically observed in spring (March) but with a lower vertical development and a stronger impact (factor 2 to 3) on the ground-level mass compared to summer. Sporadic events of biomass burning aerosols are observed in winter (January) and particularly in January 2006 when the biomass burning aerosol are advected between 1.5 and 3.5 km high. On average, the seasonal signal in the aerosol optical properties and vertical distribution is very similar from year to year over our 3 year monitoring.

Correspondence to: J.-F. Léon
(jean-francois.leon@aero.obs-mip.fr)

1 Introduction

Mineral dust emitted from arid and semi-arid regions of the Earth is a major component of the global tropospheric aerosol load, their emissions being estimated to represent about 40% of the global annual mass of aerosols emitted on Earth. All year long, massive airborne plumes of desert dust from the Sahara and surrounding regions are exported to the North Atlantic ocean (D'Almeida, 1986). African mineral dust is the dominant component in the aerosol light scattering in the North Atlantic trade winds (Li et al., 1996) and therefore exert a large forcing on the radiative budget. The instantaneous direct radiative forcing can be as large as $-129\,\mathrm{W\,m^{-2}}$ off the west African coast (Haywood et al., 2003). Since African mineral dust is composed of large super-micron particles, it also affects the radiative balance in the thermal spectrum. During the Saharan Dust Experiment (Tanré et al., 2003), the effect on irradiance due to the dust outbreak was a decrease in upwelling terrestrial radiation at the top of the atmosphere of $6.5\,\mathrm{W\,m^{-2}}$ and an increase in downwelling terrestrial radiation at the surface of $11.5\,\mathrm{W\,m^{-2}}$ (Highwood et al., 2003). Despite their large size, dust particles are transported over large distances across the Atlantic ocean (Petit et al., 2005). Depending on season the African dust reaches the northeastern coast of South America or the Caribbean Sea (Prospero and Nees, 1986). Saharan dust is transported over the ocean all year long but more abundantly during the summer months as a result of large-scale dust outbreaks. The latitudinal movement of the large-scale circulation, including the migration of the intertropical convergence zone, is responsible for the seasonal

Published by Copernicus Publications on behalf of the European Geosciences Union.

shift of the dust transport. The maximum dust transport shifts northward from ∼5° N during winter to ∼20° N during summer (Jankowiak and Tanré, 1992; Moulin et al., 1997). These dust outbreaks are mostly confined to a deep mixed layer, commonly referred to as the Saharan Air Layer (Karyampudi et al., 1999; Prospero and Carlson, 1972). However, ground observations performed at Cape Verde Islands (Chiapello et al., 1995) indicate that a low-level dust transport occurs in the trade wind layer during the winter period. This wintertime transport has also been observed from Lidar sounding in Cape Verde in January 2008 (Tesche et al., 2009). In autumn (September) Léon et al. (2003) have observed a two-layer vertical structure dust transport during the Saharan Dust Experiment. A first layer of ∼1 km thick was located within the sub-Saharan transition layer and the aloft layer was between 2 and 5 km within the Saharan Air Layer. Analysis of lidar and satellite data (Léon et al., 2003) and aircraft in situ samplings (Formenti et al., 2003) indicate that the size of the particle within the two dust layers was significantly different and that this difference might be explained be the different origin of each layer. The most western tip of Africa, the Dakar peninsula, is ideally located for a monitoring of the export of aerosols to the Atlantic Ocean, as it is on the way of major dust outbreaks. Moreover it is also affected by the advection of biomass burning aerosols coming from Sub-Sahelien tropical forests during wintertime. The biomass burning in Northern Africa follows a well-known seasonal cycle that is also controlled by the latitudinal oscillation of the inter-tropical convergence zone. Maximum emission of biomass burning aerosols in the sub-Sahelien region of North Africa occurs during December–February (Haywood et al., 2008). It results that the western tip of Africa is influenced by different type of aerosols as a function of the time of the year: biomass burning aerosols during winter and dust during spring-summer. The contribution of urban/industrial aerosols is also significant in this area because of the proximity of large urban centers in western Africa. However the emissions from megacities in Africa are not still well estimated.

This paper focuses on the monitoring of aerosol optical properties and vertical structure using Sun photometer and lidar observations at the site of M'Bour, Senegal (16.96° W; 14.39° N), located at the westernmost tip of Africa. The ground-based measurements used in our analysis have been acquired in the context of the AMMA (African Monsoon Multidisciplinary Analysis) international campaign, deploying instruments over several sites of North West Africa (Redelsperger et al., 2006; Haywood et al., 2008). Four AMMA super stations have been selected for a comprehensive investigation of aerosol properties, along with radiation measurements (Banizoumbou – Niger, Djougou – Benin, Tamanrasset – Algeria, and M'Bour – Senegal). The M'Bour site is located in an area where the contribution of biomass burning aerosol is expected to be significant, in addition to mineral dust influence (Haywood et al., 2008; Derimian et al., 2008). A special observing period has been established for the dry season (SOP0, January–February 2006), with a focus on aerosol chemical, physical, and optical properties and the associated radiative effects (Haywood et al., 2008; Chou et al., 2008; Derimian et al., 2008; Mallet et al., 2008; Pelon et al., 2008; Rajot et al., 2008; Heese and Wiegner, 2008). One of the primary aims of this SOP-0 was to document both mineral dust (mostly natural) and anthropogenic biomass burning aerosol, and their interactions over the North West Africa region. The analysis presented here relies on Lidar, Sunphotometer, and TEOM measurements performed in M'Bour over a longer duration (2006–2008) in order to investigate aerosol patterns over several seasons. The objective is to document the seasonal variability of aerosol radiative properties, mass and vertical distribution over 3 years. We first introduce the instrumentation set-up at M'Bour and the methodology used. We then present the radiative properties of the columnar aerosols and then their vertical distribution in term of extinction coefficient and altitude of the layers.

2 Instrumentation and methodology

In the frame of the AMMA experiment, all the instruments have been installed at the geophysical station of the Institut de Recherche pour le Développement (IRD center) in M'Bour, 80 km south of Dakar (Derimian et al., 2008). The site is located close to the sea shore and is affected by the sea breeze and the advection of maritime aerosols in the boundary layer.

The instruments are set up on the roof of a 12 m high building. The aerosol mass concentration was recorded on top of the building using a Tapered Element Oscillation Microbalance (TEOM) and PM_{10} head at a 5-min time step. Temperature, wind intensity and direction, and relative humidity were also monitored on site. The site is equipped with an automatic Sun photometer manufactured by CIMEL (see Holben et al., 1998, for all the instrument characteristics). The Sun photometer was operating from December 1996 to March 1998, from June 2000 to August 2001 and from December 2001 to May 2002. Since May 2003, the Sun photometer is working continuously and so we consider the years from 2003 to 2008 in the climatology. The total number of daily AOT observations for the period 2006–2008 is 990 (around 330 days per year) while it is 535 for the almucantar retrievals. In our analysis we have used level 1.5 data and the version 2 of the direct Sun algorithm and the sky brightness inversion (Dubovik et al., 2006). The aerosol optical thickness (AOT) is retrieved at 440, 500, 675, 870 and 1020 nm from the measurement of the Sun irradiance direct attenuation (Holben et al., 2001). To be consistent with the lidar data, the AOT is interpolated at 532 nm according to the Angström law and using 440 and 675 nm measurements. The size distribution, refractive index, single scattering albedo and phase function are retrieved from the sky brightness observation in the Almucantar according to the

method of Dubovik and King (2000) and Dubovik et al. (2002). For available Sun photometer inversions, the particle extinction-to-backscatter ratio, L_{aer} (hereinafter referred as the lidar ratio) is estimated using the Sun photometer-derived phase function at a scattering angle of 180°, $P(\pi)$ and the single scattering albedo, ω_0 at 440 and 675 nm and linearly interpolated at 532 nm.

$$L_{\mathrm{aer}}^{\mathrm{phot}}=\frac{4\,\pi}{\omega_0 P(\pi)} \tag{1}$$

The lidar system has been set up in December 2005 at M'Bour. The system is a 532 nm micro-pulse backscattering lidar manufactured by CIMEL (Pelon et al., 2008). It is an eye-safe system emitting 8 μJ pulse of light with a frequency of 4.7 kHz. The duration of the pulse is 100 ns leading to a vertical resolution of 15 m. The lidar is operating for a period of 10 mn every 20 mn and we store 1 mn-averaged profiles. In the next, we consider hourly means. The instrument has been working continuously from 22 January to 24 November 2006 and from 2 February 2007 to 12 September 2008. Some problems in the detection system have been identified in late April and May, August and October 2006 and the corrupted data have been removed from the dataset. The data processing includes the correction of the sky background noise, the correction of the spurious signal due to the detection of the scattered light in the receiver, called afterpulse effect, and the correction of the overlap function (Pelon et al., 2008). The lidar signal can be used starting from R_{min}=225 m because of the afterpulse. The sky background noise is estimated by taking the average of the signal in the far field above 22 km where there is no more contribution from the laser. The raw lidar profiles are range corrected and an overlap correction function is applied. This function is estimated from a serie of horizontal shots when the atmosphere is stable. The lidar equation for the range corrected and energy normalized attenuated backscattering coefficient $S(R)$, where R is the range, is written

$$S(R)=C\beta(R)\exp\{-2\int_0^R \alpha(r)\,dr\} \tag{2}$$

$\beta(R)$ and $\alpha(R)$ are the range dependant volume backscattering and extinction coefficient, respectively. We consider separately the contribution of the molecules (subscript "mol") from the contribution of aerosol (subscript "aer").

$$\alpha(R)=\alpha_{\mathrm{aer}}(R)+\alpha_{\mathrm{mol}}(R) \tag{3}$$

$$\beta(R)=\beta_{\mathrm{aer}}(R)+\beta_{\mathrm{mol}}(R) \tag{4}$$

β_{aer} is retrieved from the attenuated lidar backscattering coefficient following Fernald (1984) method (also known as Klett, 1981, method).

$$\beta_{\mathrm{aer}}(R)+\beta_{\mathrm{mol}}(R) = \frac{S(R)\exp\{-2\int_{R_0}^R [L_{\mathrm{aer}}(r)-L_{\mathrm{mol}}]\beta_{\mathrm{mol}}(r)\,dr\}}{\frac{S(R_0)}{\beta_{\mathrm{aer}}(R_0)+\beta_{\mathrm{mol}}(R_0)}-2\int_{R_0}^R L_{\mathrm{aer}}(r)\;S(r)\;T(r,R_0)\,dr} \tag{5}$$

where

$$L_{\mathrm{aer}}(R)=\frac{\alpha_{\mathrm{aer}}(R)}{\beta_{\mathrm{aer}}(R)} \tag{6}$$

and

$$T(r,R_0)=\exp\{-2\int_{R_0}^r [L_{\mathrm{aer}}(r')-L_{\mathrm{mol}}(r')]\beta_{\mathrm{mol}}(r')\,dr'\} \tag{7}$$

The upper range R_0 is taken between 6.5 and 7.0 km where the aerosol contribution is negligible compared to the molecular one. At this altitude, we do not detect any significant change in the backscattered lidar power that can be attributed to high altitude aerosols. Observations from the CALIPSO spaceborne lidar shows that on average the dust altitude is 4 km over the Atlantic ocean (Liu et al., 2008a). Over source regions, the observed maximum altitude over is 6.6 km and the top altitude drops as the dust moves eastward over the Atlantic ocean (Liu et al., 2008b).

As opposite to the particle lidar ratio L_{aer}, the molecular lidar ratio is constant $L_{\mathrm{mol}}=8\pi/3$ sr. The lidar ratio cannot be derived from our lidar measurements and we have to assume an effective and vertically constant value to solve Eq. (5).

We have used the aerosol optical thickness measured by the Sun photometer as a constrain to fix the effective lidar ratio (Chazette, 2002). The lidar-derived aerosol optical thickness is indeed a monotonic function of the lidar ratio used in the inversion (Pelon et al., 2002; Chazette, 2002). The aerosol optical depth is estimated from the lidar derived extinction profile using Eq. (8). The extinction profile is derived following an iterative procedure based on a simple dichotomy where the lidar ratio can vary between 10 to 100 sr. The procedure ends when τ_{aer} for a given effective lidar ratio is close (±10%) to the aerosol optical depth given by the Sun photometer. The profile is not inverted when the dichotomy procedure does not converge within a few (8 maximum) steps. It can be due to large optical thickness (typically above 2) when the lidar beam can not go through the dust layer as it was the case on 9, 10 and 11 March 2006 during a large dust event (Slingo et al., 2006). The main sources of uncertainties in the retrieval come from the unknown lidar ratio profile, the uncertainty in the reference signal $S(R_0)$, the error in the overlap function and the missing first 255 m. The effective lidar ratio used in the iterative procedure is found to be on average 20% lower than the Sun photometer derived one. The effective lidar ratio is affected by the choice of the reference signal (Chazette, 2002). The reference signal uncertainty depends on signal to noise ratio at the given altitude (which depends on the transmission below that altitude) and on the possible occurance of residual aerosols or clouds. In the bottom layer, the uncertainty in the overlap function is the primary source of error. The overlap function is estimated using the procedure explained by Pelon et al. (2008). We performed horizontal observations for clear (low optical depth) conditions and the overlap function is derived using the slope method (Kunz and de Leeuw, 1993). The overlap

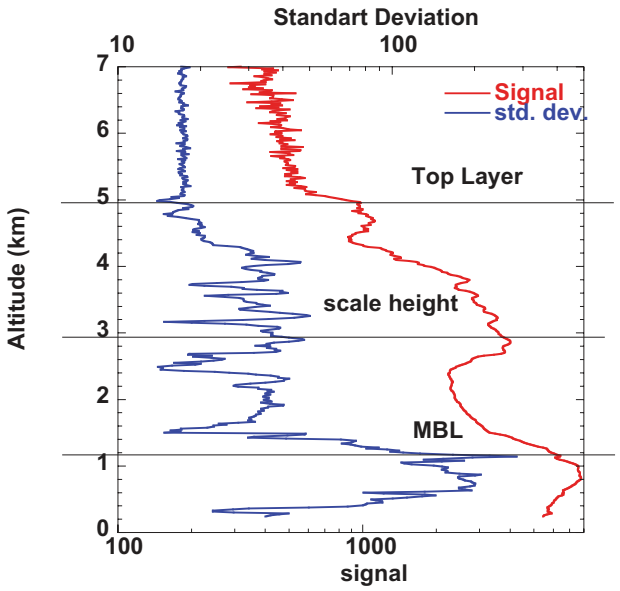

Fig. 1. Mean range corrected attenuated lidar signal (red solid line) and standart deviation (blue solid line) on 4 February 2006 at 08:00 UTC. The AOT is 0.33.

function is complete (100%) at 2 km. The correction remains large (20% of overlap) up to 600 m and the error is about 10% above 600 m while it is up to 50% close to the ground. The missing first 225 m introduces a positive bias in the retrieved extinction profile that depends on the aerosol vertical distribution and is on average 10%.

$$\tau^*_{\text{aer}} = \int_{R_{\min}}^{R_0} \alpha_{\text{aer}}(R)\, dR \tag{8}$$

We have also considered two characteristic altitudes: The top altitude of the mixed boundary layer (MBL) and the top altitude of the aloft layer (Top Layer, TL). The entrainment zone at the top of the MBL is characterized by a strong turbulent mixing that corresponds to short term fluctuations in the lidar signal. The mean and standart deviation of the lidar signal are computed every 1 h. The MBL top corresponds to the absolute maximum in the standart deviation profile (Hooper and Eloranta, 1986). The uppermost aerosol layer is also characterized by a short-term variability in the lidar signal but much weaker than for the MBL. It was not clear from the 1 h standard deviation that we can detect robustly the top aloft aerosol layer. We thus detect the top layer altitude by applying a threshold on the lidar signal itself. The average and standart deviation of the signal at the aerosol-free reference altitude between 6.5 and 7.0 km is computed. We retain the first altitude below R_0 where the signal exceeds the average by more than 3 times the standard deviation in the reference altitude. This empirical threshold is found to be a good compromise to detect the uppermost significant change in the lidar backscattering signal due to the presence of elevated aerosols as it is illustrated in Fig. 1. This figure illustrates the increase in the lidar signal and the slight decrease in the 1 h lidar signal standart deviation (at 4.98 km) at the top of the dust layer. The maximum in the 1h standart deviation profile is located at the MBL top at 1.14 km. In the case study presented in Fig. 1, the total AOT is 0.33 and the MBL AOT corresponds to 27% of the total AOT.

Moreover, a simple characterization of the profile can be given by taking the AOT scale height, H_{aer} (see Eq. 9). The aerosol optical thickness vertical profile corresponds to the vertical integration of the extinction profile, starting from the reference altitude (as defined in Eq. 8 but for any given altitude from R_0 to $R_{\min}$). So it decreases with increasing altitude. H_{aer} is the altitude at which 1/e (roughly 63%) of the total AOT is below this point (Turner et al., 2001). The scale height of background aerosols is generally assumed to be 2 km, while it is 8 km for air molecules (Seinfeld and Pandis, 1998). Even though the AOT profile does not not follow a simple exponential decay with altitude, the scale height is a good proxy for the vertical extent of the aerosols and a characteristic of the aerosol vertical mixing in the low troposphere. Considering the aforementioned sources of uncertainty in the extinction coefficient retrieval, the uncertainty in H_{aer} is expected to be less than 20%. For the case study in Fig. 1, the scale height is 2.97 km.

$$\tau_{\text{aer}}(z) = \tau^*_{\text{aer}} \exp\left(-\frac{z}{H_{\text{aer}}}\right) \tag{9}$$

The ground-level aerosol mass concentration M can be estimated from the columnar AOT and the scale height by using

$$M = \frac{\omega_0 \tau^*_{\text{aer}}}{\sigma\ H_{\text{aer}}} \tag{10}$$

where σ is the mass scattering efficiency of the bulk aerosol.

3 Seasonal pattern of the aerosol radiative properties and ground-level mass

3.1 Aerosol optical thickness

As an extensive parameter, the AOT directly depends on the total mass of the aerosol even though it also depends on the size and refractive index of the particles. On Fig. 2, the monthly average AOT for the period 2003–2008 displays a clear seasonal pattern with maxima in spring (March) and in summer (June). From May to September, the AOT is above 0.5 with maxima in June (0.65) and July (0.62), corresponding to a paroxysm in the dust outbreak activity. The AOT is continuously decreasing on average from June to December. The minimum is reached in November and December with AOT below 0.4. Figure 2 also presents the monthly mean difference for each year compared to the 2003–2008 period. The yearly average AOT in 2006 is 0.47, 0.49 in 2007 and 0.44 in 2008, while it is 0.49 for the period

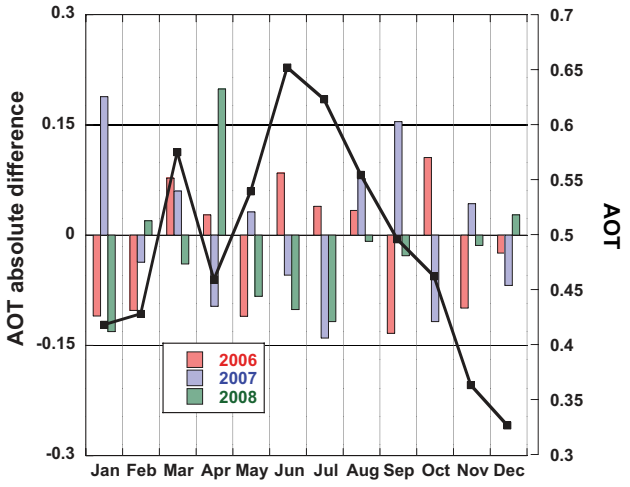

Fig. 2. Monthly mean AOT for the period 2003–2008 (black solid line). Monthly difference between (red bars) 2006, (blue bars) 2007 and (green bars) 2008 and the 2003–2008 average.

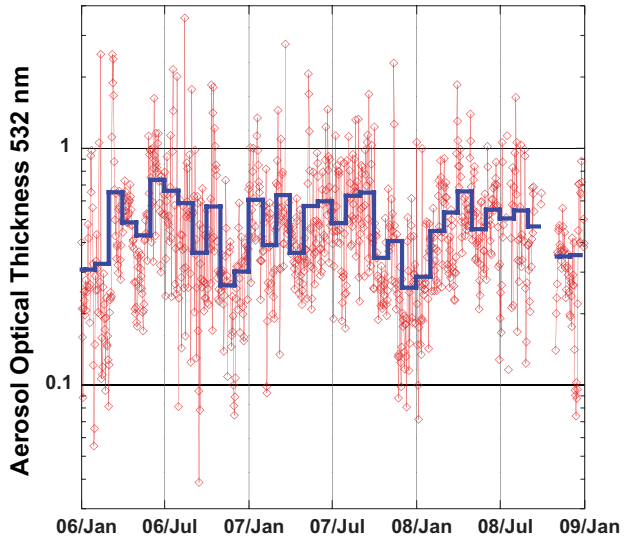

Fig. 3. Daily mean Sun photometer aerosol optical thickness estimated at 532 nm from 2006 to 2008. The blue solid line is the monthly average.

2003–2008. January 2007, April 2008 (excess of 40%) and September 2007 are well above the average AOT while January 2008, July 2007 and September 2006 are below the average. The difference between the three years remains low during the spring dust pick in March. In June, the year 2006 shows an excess in AOT while 2007 and 2008 are below the average. 2006 is below the average (around −20%) for January, February, May, September and October.

The daily variation in AOT during 2006–2008 is presented in Fig. 3 on a logarithmic scale. The AOT is variable from day to day with several peaks over 1, but we can see a

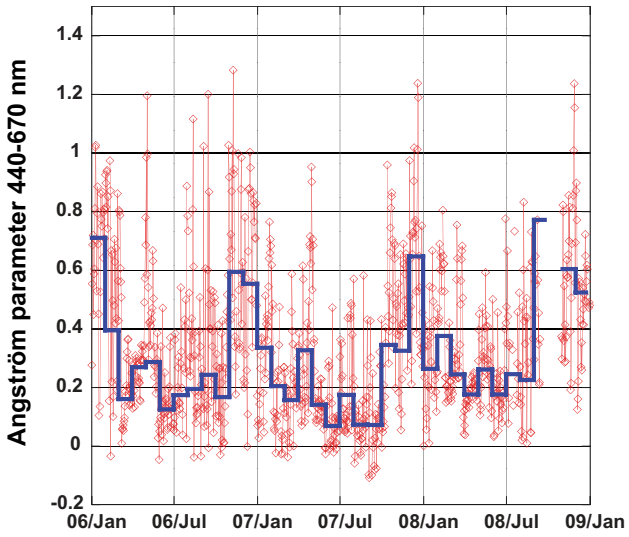

Fig. 4. Daily mean Sun photometer Angström exponent calculated between 440 and 675 nm from 2006 to 2008. The blue solid line is the monthly average.

seasonal cycle with maxima in June–July. AOT up to 2.5 are observed in March 2006, corresponding the large dust event of 7–13 March (Slingo et al., 2006; Tulet et al., 2008). Similar large sporadic events are observed in spring 2007 and 2008. Large events with a AOT above 1 occurs all year long with a maximum frequency in summer months, leading to a noisy day-to-day pattern.

3.2 Angström exponent and coarse fraction

The Angström exponent is derived from the direct AOT measurements at 440 and 675 nm. This parameter is primarily related to the size of the particles. The Angström exponent of coarse dust particles is close to 0.0 while it is close to 2.0 for submicron particles. The mixing between both type of particle tends to change the Angström exponent between those two extrema (Hamonou et al., 1999). A variation in the transport regime and physical processes occuring the transport (like sedimentation of coarser particles or particle aging; Müller et al., 2007b) might also explain a change in the size distribution and then in the Angström exponent. Figure 4 shows the variation of the Angström exponent between 2006 and 2008. The monthly average values are below 0.7 (except for January 2006 and September 2008), indicating that coarse particles are the dominant contributor to the AOT. The same feature can be also observed in the volume coarse fraction (Fig. 5) trend. Most of the time, the coarse fraction is above or close to 90%. During winter time, there is a large day-to-day variability and the monthly average value drops below 90% in association with a increase in the Angström parameter above 1.0.

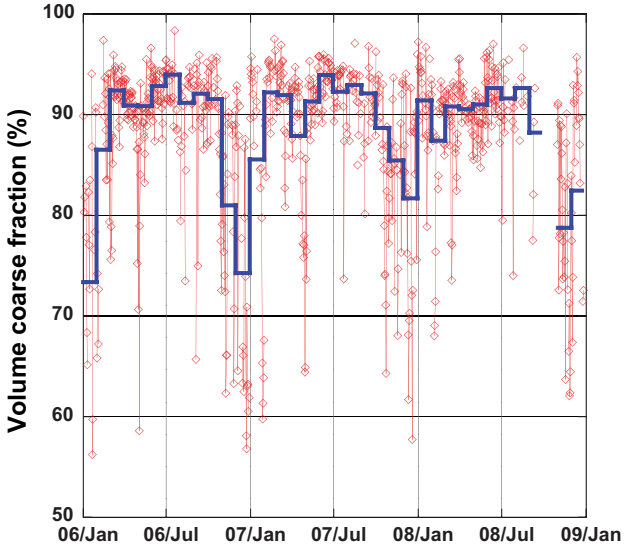

Fig. 5. Daily mean Sun photometer derived coarse fraction from 2006 to 2008. The blue solid line is the monthly average.

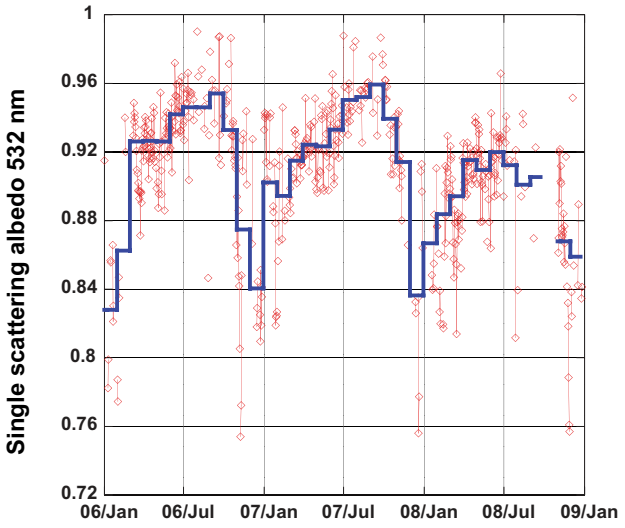

Fig. 6. Daily mean Sun photometer single scattering albedo estimated at 532 nm from 2006 to 2008. The blue solid line is the monthly average.

The variation in the Angström exponent and in the coarse mode fraction between spring and summer could reveals a change in the aerosol size distribution that can be also attributed to the change in the source area and the transport regimes.

3.3 Single scattering albedo

The seasonal trend in the single scattering albedo (SSA) is very smooth although there is a significant day-to-day variability (Fig. 6). It is to be reminded that SSA is derived from the Almucantar measurements and then the number of observations is significantly lower than for the direct AOT and Angström parameter measurements. The SSA depends on the wavelength, the size and the complex refractive index of particles. Johnson et al. (2008) have found that "pure" dust in the area of Niamey has a SSA of 0.99 while the average value for aged biomass burning aerosols is 0.85. They derived 0.81 for "pure" biomass burning. Over M'Bour, the range in SSA varies between 0.85 and 0.95 in the monthly average while on a daily basis it reaches as low as 0.75 and as high as 0.98. The range of SSA observed in M'Bour is coherent with the airborne observations provided by Osborne et al. (2008), indicating that M'Bour is under the influence of a mixture of biomass-burning and dust aerosols. During the SAMUM 2006 experiment (Heintzenberg, 2009) in Morocco, Schladitz et al. (2009) have also reported a dust SSA between 0.89±0.02 and 0.96±0.02 for conditions of low and hight dust load, respectively.

The SSA remains surprisingly low during March when the spring dust events occurs. Minima are observed during winter time (December) and maxima are observed during summer and autumn. There is a constant increase in the SSA from winter to autumn each year. January 2007 exhibits a much higher SSA (0.9) than January 2006 and 2008. This has to be linked with the anomaly in AOT (Fig. 2) that indicates an increase in the dust activity, leading to a higher SSA. The SSA during the summer 2008 is well below the other years. This is also linked with a deficit in AOT for this period. The delay from March to April in the spring dust events in 2008 can also be observed in the SSA.

3.4 Lidar ratio

The aerosol lidar ratio can vary widely depending on the aerosol size distribution, refractive index and shape. Observed lidar ratio determined by Raman lidar are in the range between 23 to 65 sr for typical atmospheric aerosols (Müller et al., 2007a) and can go up to 100 sr. The lidar ratio estimated from the Sun photometer observations shows also a clear seasonal pattern (Fig. 7). Few points are below 30 sr that might correspond to clean maritime aerosols (Müller et al., 2007a; Omar et al., 2009). From raman lidar soundings in Niamey, Niger Heese and Wiegner (2008) have found 75 sr for elevated biomass burning aerosols and 55 sr for dust. From multiwavelength aerosol Raman lidar observations in Cape Verde, Tesche et al. (2009) derived a lidar ratio of 77 sr above 1.5 km height in a layer of mixed dust and biomass burning. This range is well within the observations in M'Bour corresponding to an influence of biomass burning aerosols in winter and dominance of dust during summer.

Cattrall et al. (2005) have presented a detailed analysis of the use of Sun photometer measurements for the estimation of the lidar ratio over the globe. They report values of $L_{\mathrm{aer}}^{\mathrm{phot}}$ of 60±8 sr for biomass burning aerosols and 42±4 sr for

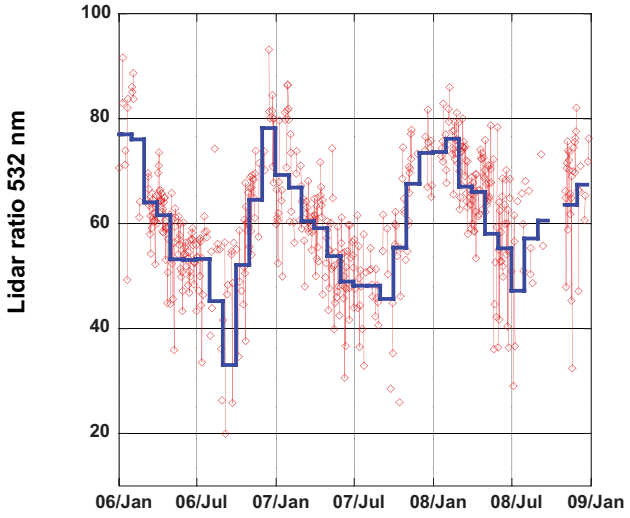

Fig. 7. Daily mean Sun photometer lidar ratio estimated at 532 nm from 2006 to 2008. The blue solid line is the monthly average.

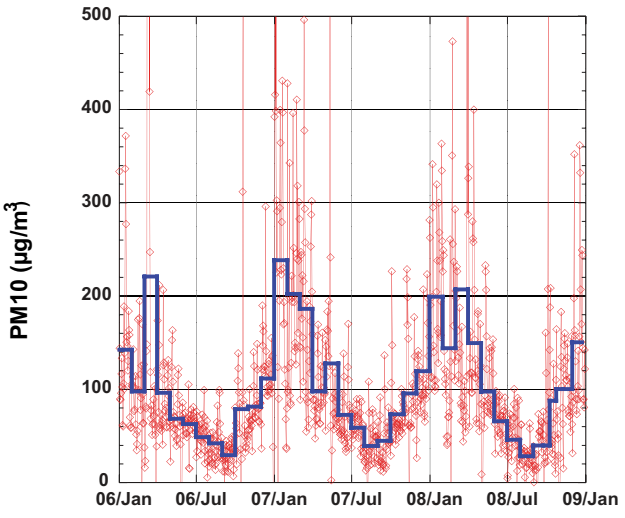

Fig. 8. Daily mean ground-level PM_{10} concentration from 2006 to 2008. The blue solid line is the monthly average.

mineral dust. The given value for biomass burning aerosols is lower than what we found but the stations selected by Cattrall et al. (2005) are located close to the biomass burning sources while the M'Bour is typically a remote station for biomass burning aerosols. In 2006 and 2007, a quasi-linear decrease from January to September can be observed starting from 76 sr to 32 sr (2006) and 45 sr (2007). As opposite, 2008 looks atypical. The minimum is observed in July while it is in September for 2006 and 2007 and the maximum appears in February, not in January or December. It has to be reminded that that $L_{\text{aer}}^{\text{phot}}$ is a columnar integrated parameter and that the true lidar ratio is range dependant.

3.5 Ground-level mass

PM_{10} mass was continuously recorded on site from 2006 to 2008. Figure 8 presents the daily and monthly mean PM_{10} concentration observed at M'Bour. The minima are in September 2006 and August 2007 and 2008. As opposite to the AOT seasonal pattern (Figs. 2 and 3) the summer maximum is not observed in the ground-level PM_{10} concentration. In 2006 and 2008, March is the month with the higher concentration (more than 200 $\mu g/m^3$) while it is January in 2007. As it has been also reported by Prospero (1981), the ground-level aerosol mass is about 3 times lower in summer than in winter.

4 Vertical distribution

4.1 Seasonal variability of the extinction profiles

Figure 9 presents the monthly average extinction profiles for 2006, 2007 and 2008. The data for January 2007, October 2008, December 2006 and November–December 2008 are missing. Only 3 days are available in November 2006. We first present an analysis by considering the following season: Winter (December, January, February), Spring (March, April, May), Summer (June, July, August) and Autumn (September, October, November).

4.1.1 Winter

The data for December 2006, 2008 and January 2007 are lacking. The extinction profiles acquired in January–February 2006 show large differences compared to 2007 and 2008. A maximum in the extinction at about 1 km is observed in January and February 2008 and December and February 2007, while it is at 2 km in January 2006. A large aloft aerosol layer between 1.5 and 4.0 km is observed in January 2006 that is not observed in 2008. However the monthly average AOT is about the same, a slight difference can be observed in the SSA. In January 2006, the SSA is 0.83 while in January 2008 it is 0.87. This difference might be attributed to the presence of the aloft transport of biomass burning aerosol in the winter period (Haywood et al., 2008). In February, 2006 shows a large difference in the lower part of the extinction profile (below 3 km) compared to 2007 and 2008. February 2006 is characterized by a large anomaly in the AOT that can be attributed to a weaker low-level aerosol transport compared to the other years.

4.1.2 Spring

The month of March is very similar for the 3 years and shows low level transport with extinction coefficient close to 0.2 km^{-1} below 1.5 km. In April, the top of the dust layer is located between 4 and 5 km for the three years along with

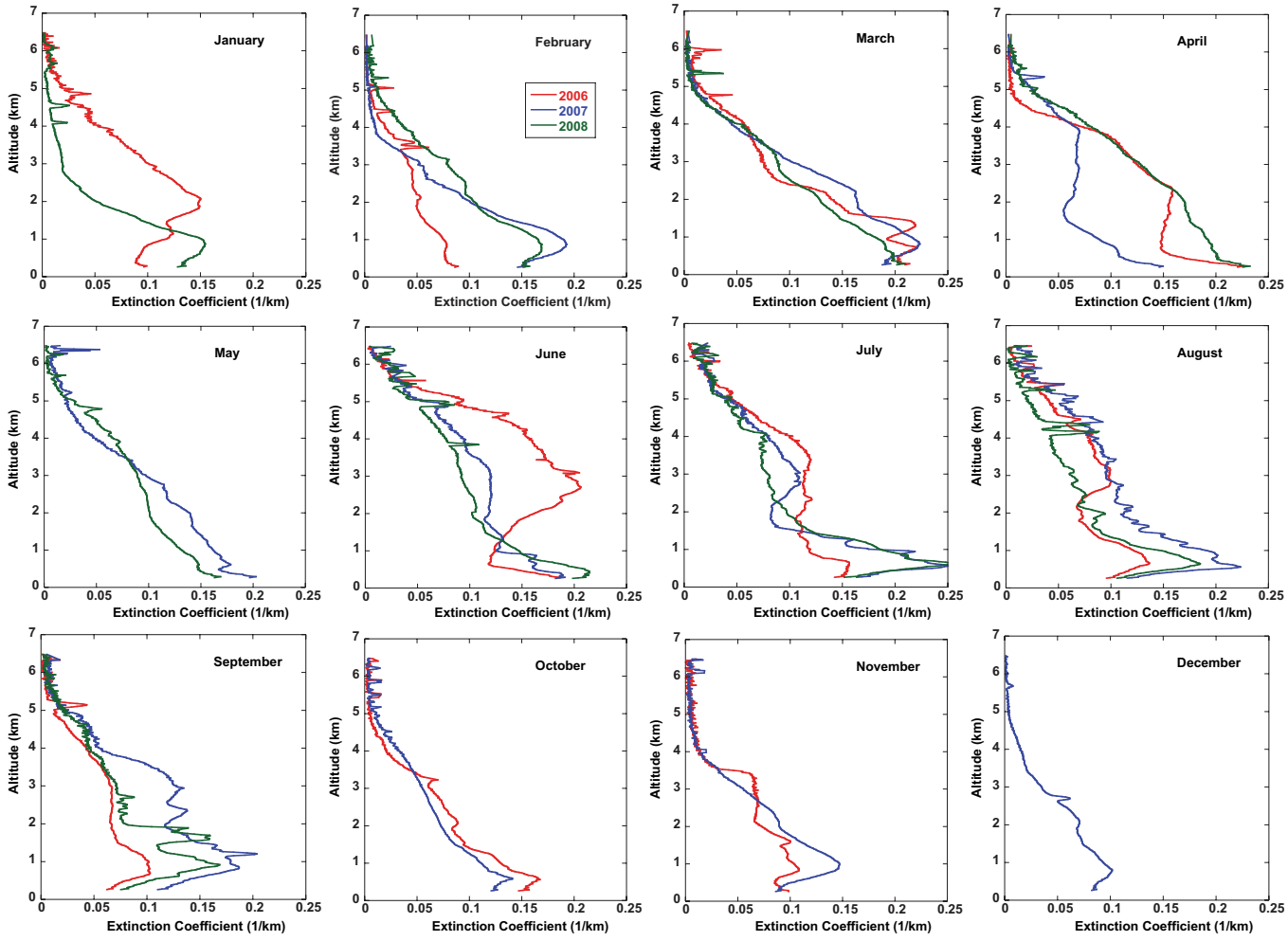

Fig. 9. Monthly average vertical profiles of aerosol extinction at 532 nm for (red solid line) 2006, (blue solid line) 2007 and (green solid line) 2008.

less extinction in the lower layer than in March, except for 2008. However there is a large variability in the extinction profile from year to year. In 2006 and 2008, the main difference in the extinction is located below 2 km that can be related to a slight change in the amount of dust advected in the lower layer. In April 2007, the extinction coefficient is significantly lower than the other years considering altitudes below 4 km.

4.1.3 Summer

In June, the main difference is observed in 2006, with an enhance dust extinction above 2 km compared to the other years. There is clearly an influence of the mineral dust events, corresponding to a decrease in the Angström coefficient (Fig. 4) and a decrease in the lidar ratio (Fig. 7). In July and August 2007–2008 show more extinction in the lower layer while 2006 shows well the dust transport in the Saharan air layer between 2 and 5 km.

4.1.4 Autumn

Autumn is clearly marked by a low level thick layer between 1 and 2 km. It is more obvious for 2007 and 2008 than for 2006. Léon et al. (2003) have also reported observations of a thick aerosol layer located between 1 and 2 km from lidar measurements between Capo Verde Islands and Dakar tip in September 2001. This layer was composed with particles having an effective radius of 0.67 μm suggesting a contribution of small particles. The profil in 2008 shows 2 maxima below 2 km. The Angström parameter is also higher than for the two other years indicating a significant contribution of small absorbing particles either from large scale or local origin, as the contribution of local pollution coming from the urban area of Dakar or close-by industries is not well know so far. The transport of dust in altitude if also more abundant in 2007.

Table 1. Average aerosol parameters corresponding to the profiles presented in Fig. 11 for the aerosol optical thickness (AOT), ground-level mass concentration (M), lidar ratio ($L_{\text{aer}}^{\text{phot}}$), single scattering albedo (SSA), Volume coarse fraction (Vc), scale height (H_{aer}), top layer altitude (H_{top}), and number of days (N). The standard deviation is given in brackets.

		AOT	M (μg/m^3)	$L_{\text{aer}}^{\text{phot}}$ (sr)	SSA	Vc (%)	H_{aer} (km)	H_{top} (km)	N
SSA<0.85	AOT<0.5	0.33 (0.08)	100 (29)	79 (12)	0.82 (0.03)	75 (9)	2.6 (0.6)	4.8 (0.4)	15
	AOT>0.5	0.62 (0.16)	144 (103)	77 (9)	0.83 (0.03)	78 (15)	2.7 (0.6)	4.8 (1.0)	7
0.85<SSA<0.95	AOT<0.5	0.39 (0.08)	104 (65)	63 (10)	0.91 (0.02)	89 (6)	2.8 (0.8)	4.7 (1.0)	166
	AOT>0.5	0.72 (0.24)	154 (194)	63 (8)	0.92 (0.02)	92 (2)	2.9 (0.7)	5.0 (1.1)	146
SSA>0.95	AOT<0.5	0.38 (0.08)	54 (31)	51 (11)	0.97 (0.01)	89 (5)	3.0 (1.1)	5.1 (0.9)	17
	AOT>0.5	0.78 (0.21)	52 (27)	51 (6)	0.96 (0.01)	93 (1)	3.4 (0.7)	5.7 (0.4)	13

4.2 Layer altitudes

As shown on Fig. 9, the high resolution aerosol extinction vertical distribution is complex. Several minima and maxima can be observed corresponding to the signature of the atmospheric dynamic and aerosol source activity. It is then a rather difficult task to characterize the extinction distribution by any given number. During daytime, the lower part of the troposphere can be separated into two parts: the mixed boundary layer (MBL) and the free troposphere. We have monitored the top altitude of MBL and the dust layer (referred as top layer, TL) within the free troposphere. Figure 10 shows the monthly mean altitude for the TL, and daily maximum top altitude of the MBL. There is a very clear seasonal signal in the TL with maxima in summer and minima in winter oscillating between 2.8 and 5.8 km. The maximum is reached in June for the years with an altitude above 5.0 km in coincidence with the paroxysm in the dust activity. The MBL altitude ranges between 1.2 and 1.7 km. There is not a clear seasonal signal in the MBL altitude. However maxima are observed in August or September in agreement with the seasonal pattern of the surface temperature (not shown).

The scale height provides an additional information on the vertical mixing of aerosols. In general, the seasonal variation in the scale height is very similar to the one for the top altitude. It is about 3.0 km in summer and 1.8–2.0 km in winter. When the scale height decreases but the top of the layer remains the same, it indicates that an additional low level aerosol transport occurs as it is the case in July 2007. This is in conjunction with the lower thick layer (Fig. 9) that appears in July 2007. Over the 3 years, the scale height tends to slightly decrease.

4.3 Vertical profiles by aerosol types

Atmospheric aerosols can be classified according to their intrinsic optical properties. We have considered profiles for which the columnar SSA is below 0.85 (biomass burning aerosols) or above 0.95 (mineral dust) and made the distinction when the AOT is below or above 0.5. Table 1 presents

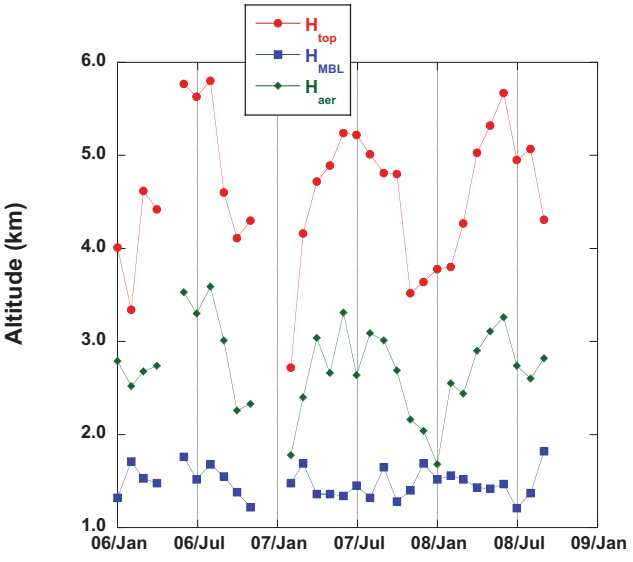

Fig. 10. Monthly mean top altitude of the (red) upper most layer and (blue) daily maximum of the mixed boundary layer. The green solide line is the monthly mean scale height.

the average optical parameters for each category along with mean scale height and top altitude of the aerosol layer.

Figure 11a gives the average profiles for the pure dust cases. When the AOT is above 0.5, we can observe the Saharan Air Layer corresponding to a dust layer between 2 and 6 km and with a maximum extinction coefficient of 0.2 km^{-1}. The average lidar ratio is 51±6 sr and the volume coarse fraction is 93 %. It corresponds also to a low (52 μg/m^3) PM_{10} at the ground-level highlighting that most of the dust is transported in the aloft layer. Such vertical structure of the dust transport has also been observed by Berthier et al. (2006) from the LITE spaceborne lidar over the Tropical Atlantic Ocean off the western African coast.

Figure 11b presents the biomass burning aerosol profiles (SSA below 0.85). There is not a drastic change in the shape of the vertical profile when the AOT is above or below 0.5. The volume coarse fraction is below 80% and the lidar ratio

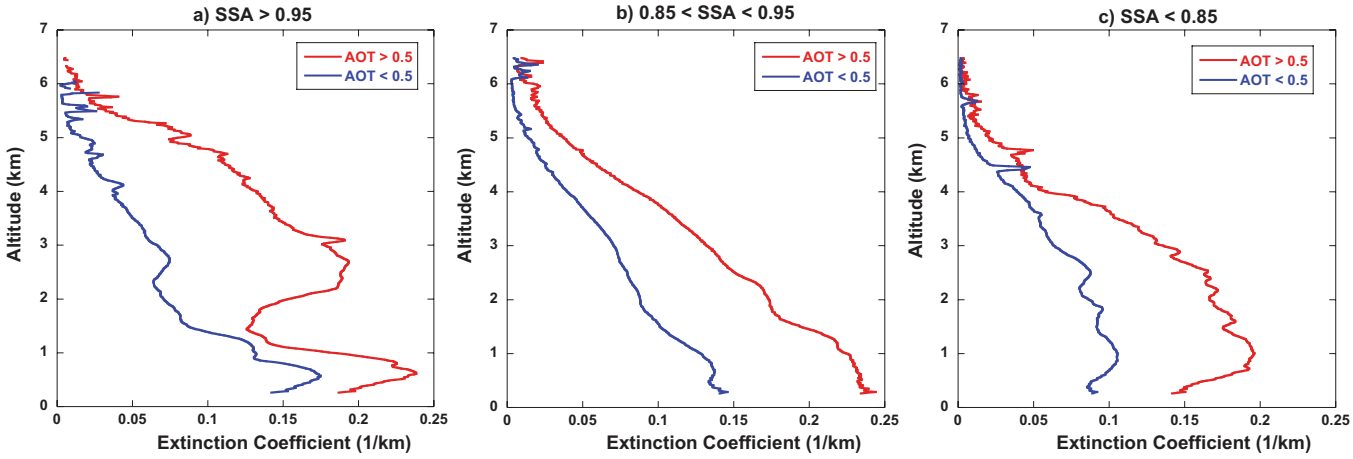

Fig. 11. Average profile corresponding to **(a)** SSA>0.95, **(b)** 0.85<SSA<0.95 and **(c)** SSA<0.85. The blue and the red line corresponds to profiles having a columnar AOT below or above 0.5, respectively.

is 77±9 sr when the AOT is above 0.5. The biomass burning aerosols are located in a 3 km thick layer which extends to about 4 km. The average PM_{10} at the ground is much higher than in the pure dust case in agreement with the lower altitude transport (indicated in Table 1 by the scale height and the top layer altitude). In Cape Verde, Tesche et al. (2009) have shown that this thick layer is mixed of dust and biomass burning aerosols with a relative contribution to the total extinction of 1/3 and 2/3 respectively.

In most cases, the SSA is between 0.85 and 0.95 and the average profiles (Fig. 11c) corresponds to a mix of high and low aerosol layers. When the AOT is above 0.5, the extinction coefficient in the bottom layer (below 2 km) is high in conjunction with high PM_{10} at the ground-level. This is characteristic of the spring dust transport occurring in March, corresponding also to a high volume coarse fraction (92%, see Table 1).

4.4 Comparison with aerosol mass

During summer and winter, the ground-level PM_{10} is not correlated to the AOT even when the scale height is accounted for (see Eq. 10). The highest correlation was found in March, when the dust is transport close to the ground. Figure 12 shows the comparison between the daily mean ground-level aerosol mass and $\omega_0 \tau^*_{aer} / H_{aer}$ in March 2006, 2007 and 2008. Data point with coincident almucantar measurements have been selected. The coefficient correlation R^2 is 0.76. The linear fit yields a mass scattering efficient of 0.81±0.03 m^2/g. This value is in a good agreement with the 1.1±0.4 m^2/g for total dust given by Hand and Malm (2007) in their general review of mass scattering efficiency.

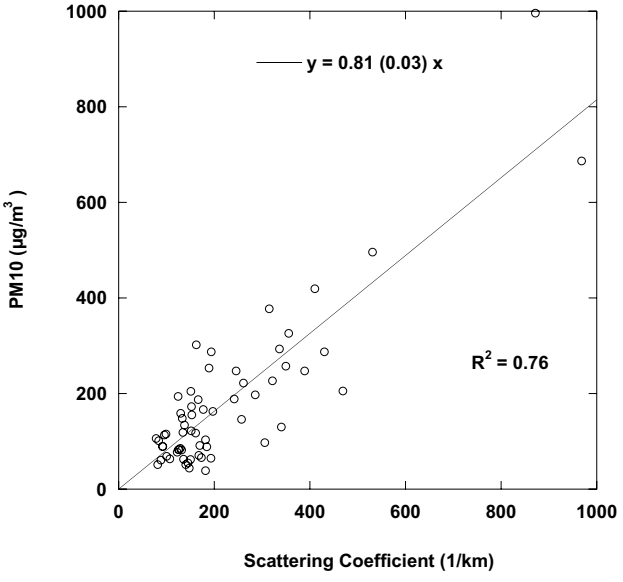

Fig. 12. Comparison between lidar derived scattering coefficient and ground-level PM_{10} using data acquired in March 2006, 2007 and 2008.

5 Discussion and conclusions

For the first time, we have obtained a monitoring of the dust transport and optical properties over 3 years at the westernmost tip of the African continent. This place of the world is all year long affected by the export of mineral dust as it moves westward to the north Atlantic ocean. The mineral dust export is mainly driven by the longitudinal oscillation of the inner-tropical discontinuity (Schepanski et al., 2009). The main feature is a northward shift of the dust plume and an increase in the altitude of the layers during

summer months compared to wintertime. In the summer months, M'Bour is under the influence of major Saharan dust sources. The contribution of dust being then dominant, it implies a single scattering albedo above 0.95 and an AOT above 0.5. During this period, we have observed the Saharan air layer that corresponds to a thick dust layer between 2 and 6 km and corresponding to about 70% of the total AOT. A decrease in the AOT scale height is observed in the late summer corresponding to the presence of an additional bottom layer (up to 2.0 km) in agreement with the previous observations of Léon et al. (2003) and Karyampudi et al. (1999). In winter, the site is less affected by dust which is transported southward toward the Gulf of Guinea by the northeasterly winds (Kalu, 1979). The monitoring site is also under the influence of tropical biomass burning aerosol emissions as it is reveals by the seasonal pattern of the aerosol optical properties. The altitude of the biomass burning aerosol layer can reach up to 4 km in January or February and is characterized by a columnar single scattering albedo below 0.85. Most of the time, this latter parameter is between 0.85 and 0.95 indicating a mixing of absorbing and scattering aerosols that occurs in the lower layer below 2 km. The PM_{10} mass measured at the ground level catches well the spring dust events in March but is not affected by the summer dust transport that occurs in altitude. In March, it was possible to estimate that the mass scattering efficiency is $0.81 \pm 0.03\ m^2/g$.

More than 30 years ago, the seasonal pattern of the dust transport to the Atlantic ocean was investigated on the basis of field experiments (Kalu, 1979; Prospero and Carlson, 1972). In this study, we provide a long-term vertical profile aerosol monitoring in West Africa. Our 3 year analysis confirms the main features of the winter and summer dust vertical stratification. Moreover, we quantify the seasonal variability of the aerosol extinction in the different layers. The optical properties also reveals the influence of the biomass burning aerosols during the winter season. From our 3 year intensive monitoring, it is not possible to conclude on the inter-annual variation in the dust optical properties or altitude. It is then necessary to extent the monitoring to further understand the possible links between the characteristic of the dust transport and climate change in Africa.

Acknowledgements. Based on a French initiative, AMMA was built by an international scientific group and is currently funded by a large number of agencies, especially from France, UK, US and Africa. It has been the beneficiary of a major financial contribution from the European Community's Sixth Framework Research Programme. Detailed information on scientific coordination and funding is available on the AMMA International web site http://www.amma-international.org. The authors are very thankful to Tamsir Diop and the staff of the Institut de Recherche pour le Développement for their involvement in setup and management of the site. The authors are very thankful to P. Goloub and B. Holben and all the members of the AERONET and PHOTONS groups for managing the Sun photometer network and providing high quality data.

Edited by: P. Formenti

The publication of this article is financed by CNRS-INSU.

References

Berthier, S., Chazette, P., Couvert, P., Pelon, J., Dulac, F., Thieuleux, F., Moulin, C., and Pain, T.: Desert dust aerosol columnar properties over ocean and continental Africa fom Lidar in Space Technology Experiment, J. Geophys. Res, 111, D21202, doi:10.1029/2005JD006999, 2006.

Cattrall, C., Reagan, J., Thome, K., and Dubovik, O.: Variability of aerosol and spectral lidar and backscatter and extinction ratios of key aerosol types dervied from selected Aerosol Robotic Network locations, J. Geophys. Res., 110, D10S11, doi:10.1029/2004JD005124, 2005.

Chazette, P.: The monsoon aerosol extinction properties at Goa during INDOEX as measured with lidar, J. Geophys. Res., 108(D6), 4187, doi:10.1029/2002JD002074, 2003.

Chiapello, I., Bergametti, G., Gomes, L., Chatenet, B., Dulac, F., Pimenta, J., and Santos Suares, E.: An additional low layer transport of Sahelian and Saharan dust over the north-eastern tropical Atlantic, Geophys. Res. Lett., 22, 3191–3194, 1995.

Chou, C., Formenti, P., Maillé, M., Ausset, P., Helas, G., Osborne, S., and Harrison, M.: Size distribution, shape and composition of dust aerosols collected during the AMMA SOP0 field campaign in the northeast of Niger, January 2006, J. Geophys. Res., 113, D00C10, doi:10.1029/2008JD009897, 2008.

D'Almeida, G. A.: A model for Saharan dust transport, J. Clim. Appl. Meteorol., 25, 903–916, 1986.

Derimian, Y., Léon, J.-F., Dubovik, O., Chiapello, I., Tanré, D., Sinyuk, A., Auriol, F., Podvin, T., Brogniez, G., and Holben, B.: Radiative properties of aerosol mixture observed during the dry season 2006 over M'Bour, Senegal (African Monsoon Miltidisciplinary Analysis campaign), J. Geophys. Res., 113, D00C09, doi:10.1029/2008JD009904, 2008.

Dubovik, O. and King, M.: A flexible inversion algorithm for retrieval of aerosol optical properties from sun and sky radiance measurements, J. Geophys. Res., 105, 20673–20696, 2000.

Dubovik, O., Holben, B., Lapyonok, T., Sinyuk, A., Mishchenko, M., Yang, P., and Slutsker, I.: Non-spherical aerosol retrieval method employing light scattering by spheroids, Geophys. Res. Lett., 29, 10, doi:10.1029/2001GL014506, 2002.

Dubovik, O., Sinyuk, A., Lapyonok, T., Holben, B., Mishchenko, M., Yang, P., Eck, T., Volten, H., Munoz, O., Veihelman, B., Van der Zand, W., Léon, J.-F., Sorokin, M., and Slutsker, I.: The application of spheroid models to account for aerosol particle non sphericity in remote sensing of desert dust, J. Geophys. Res., 111, D11208, doi:10.1029/2005JD006619, 2006.

Fernald, F.: Analysis of atmospheric lidar observations: Some comments, Appl. Optics, 23, 652–653, 1984.

Formenti, P., Elbert, W., Maenhaut, W., Haywood, J., and Andreae, M.: Chemical composition of mineral dust aerosol during the Saharan Dust Experiment (SHADE) airborne campaign in the Cape Verde region, September 2000, J. Geophys. Res., 108, 8576, doi:10.1029/2002JD002648, 2003.

Hamonou, E., Chazette, P., Balis, D., Dulac, F., Schneider, X., Galani, E., Ancellet, G., and Papayannis, A.: Characterisation of the vertical structure of Saharan dust export to the Mediterranean bassin, J. Geophys. Res., 104, 22257–22270, 1999.

Hand, J. and Malm, W.: Review of aerosol mass scattering efficiencies from ground-based measurements since 1990, J. Geophys. Res., 112, D16203, doi:10.1029/2007JD008484, 2007.

Haywood, J., Osborne, S., Francis, P., Keil, A., Formenti, P., Andreae, M., and Kaye, P.: The mean physical and optical properties if regional haze dominated by biomass burning aerosol measured from C-130 aircraft during SAFARI 2000, J. Geophys. Res., 108, 8473, doi:10.1029/2002JD002687, 2003.

Haywood, J., Pelon, J., Formenti, P., et al.: Overview of the dust and biomass burning experiment and African monsoon multidisciplinary analysis special observing period-0, J. Geophys. Res., 113, D00C11, doi:10.1029/2008JD010077, 2008.

Heese, B. and Wiegner, M.: Vertical aerosol profiles from Raman polarization lidar observatins during the dry season AMMA field campaign, J. Geophys. Res., 113, D00C11, doi:10.1029/2007JD009487, 2008.

Heintzenberg, J.: The SAMUM-1 experiment over Southern Morocco: overview and introduction, Tellus B, 61, 2–11, 2009.

Highwood, E., Haywood, J., Silverstone, M., Newman, S., and Taylor, J.: Radiative properties and direct effect of Saharan dust measured by the C-130 aircraft during the Saharan Dust Experiment (SHADE): 2. Terrestrial spectrum, J. Geophys. Res., 108, 8578, doi:10.1029/2002JD002552, 2003.

Holben, B., Eck, T., Sluster, I., Tanré, D., Buis, J., Setzer, A., Vermote, E., Reagan, J., Kaufman, Y., Nakajima, T., Lavenu, F., Jankowiak, I., and Smirnov, Z.: AERONET-A federated instrument network and data archive for aerosol characterisation, Remote Sens. Environ., 66, 1–16, 1998.

Holben, B., Tanré, D., Smirnov, A., Eck, T., Slutsker, I., Abuhassan, N., Newcomb, W., Schafer, J., Chatenet, B., Lavenu, F., Kaufman, Y., Vande Castle, J., Setzer, A., Markham, B., Clark, D., Frouin, R., Halthore, R., Karneli, A., O'Neill, N., Pietras, C., Pinker, R., Voss, K., and Zibordi, G.: An emerging ground-based aerosol climatology: Aerosol optical depth from AERONET, J. Geophys. Res., 106, 12067–12097, 2001.

Hooper, W. and Eloranta, E.: Lidar measurements of wind in the planetary boundary layer: the method, accuracy and results from joint measurements with radiosonde and kytoon, J. Clim. Appl. Meteorol., 25, 990–1001, 1986.

Jankowiak, I. and Tanré, D.: Satellite climatology of Saharan dust outbreaks: Method and preliminary results, J. Climate, 5, 646–656, 1992.

Johnson, B., Osborne, S., Haywood, J., and Harisson, M.: Aircraft measurements of biomass burning aerosol over West Africa during DABEX, J. Geophys. Res., 113, D00C06, doi:10.1029/2007JD009451, 2008.

Kalu, A.: The African dust plume: Its characteristics and propagation acress west Africa in winter, SCOPE, 14, 95–118, 1979.

Karyampudi, V., Palm, S., Reagen, J., Fang, H., Grant, W., Hoff, R., Moulin, C., Pierce, H., Torres, O., Browell, E., and Melfi, S.: Validation of the saharan dust plume conceptual model using lidar, Meteosat, and ECMWF data, B. Am. Meteorol. Soc., 80, 1045–1075, 1999.

Klett, J.: Stable analytical inversion solution for processing lidar return signal, Appl. Optics, 20, 211–220, 1981.

Kunz, G. and de Leeuw, G.: Inversion of lidar signals with the slope method, Appl. Optics, 32, 3249–3256, 1993.

Léon, J.-F., Pelon, J., Tanré, D., Kaufman, Y., Goloub, P., Haywood, J., and Chatenet, B.: Profiling of a Saharan dust outbreak based on a synergy between active and passive remote sensing, J. Geophys. Res., 108, 8575, doi:10.1029/2002JD002774, 2003.

Li, X., Maring, H., Savoie, D., Voss, K., and Prospero, J.: Dominance of mineral dust in aerosol scattering in the North Atlantic trade winds, Nature, 380, 416–419, 1996.

Liu, D., Wang, Z., Liu, Z., Winker, D., and Trepte, C.: A height resolved global view of dust aerosols from the first year CALIPSO lidar measurements, J. Geophys. Res, 113, D16214, doi:10.1029/2007JD009776, 2008a.

Liu, Z., Omar, A., Vaughan, M., Hair, J., Kittaka, C., Hu, Y., Powell, K., Trepte, C., Winker, D., Hostetler, C., Ferrare, R., and Pierce, R.: CALIPSO lidar observations of the optical properties of Saharan dust: A case study of long-range transport, J. Geophys. Res, 113, D07207, doi:10.1029/2007JD008878, 2008b.

Mallet, M., Pont, V., Liousse, C., et al.: Aerosol direct radiative forcing on Djougou (northern Benin) during the African Monsoon Multidisciplinary Analysis dry season experiment (SOP-0), J. Geophys. Res., 113, D00C01, doi:10.1029/2007JD009419, 2008.

Moulin, C., Lambert, C., Dulac, F., and Dayan, U.: Control of atmospheric export of dust from North Africa by the North Atlantic Oscillation, Nature, 387, 691–694, 1997.

Müller, D., Ansmann, A., Mattis, I., Tesche, M., Wandingen, U., Althausen, D., and Pisani, G.: Aerosol-type dependent lidar ratios observed with Raman lidar, J. Geophys. Res., 112, D16202, doi:10.1029/2006JD008292, 2007a.

Müller, D., Mattis, I., Ansmann, A., Wandinger, U., Ritter, C., and Kaiser, D.: Multiwavelength Raman lidar observations of particle growth during long-range transport of forest-fire smoke in the free troposphere, Geophys. Res. Lett., 34, L05803, doi:10.1029/2006GL027936, 2007b.

Omar, A., Winker, D., Kittaka, C., Vaughan, M., Liu, Z., Hu, Y., Trepte, C., Rogers, R., Ferrare, R., Lee, K.-P., Kuehn, R., and Hostetler, C.: The CALIPSO automated aerosol classification and lidar ratio selection algorithm, J. Atmos. Ocean. Tech., 26, 1994–2014, 2009.

Osborne, S., Johnson, B., Haywood, J., Baran, A., Harrison, M., and McConnell, C.: Physical and optical properties of mineral dust aerosol during the Dust and Biomass-burning Experiment, J. Geophys. Res., 113, D00C03, doi:10.1029/2007JD009551, 2008.

Pelon, J., Flamant, C., Chazette, P., Léon, J.-F., Tanré, D., Sicard, M., and Satheesh, S.: Characterization of aerosol spatial distribution and optical properties over the Indian Ocean from airborne lidar and radiometry during INDOEX'99, J. Geophys. Res., 107, 8029, doi:10.1029/2001JD000402, 2002.

Pelon, J., Mallet, M., Mariscal, A., Goloub, P., Tanré, D., Bou Karam, D., Flamant, C., Haywood, J., Pospichal, B.,

and Victori, S.: Microlidar observations of biomass burning aerosol over Djougou (Benin) during African Monsoon Multidisciplinary Analysis Special Observation Period 0: Dust and Biomass Burning Experiment, J. Geophys. Res., 113, D00C18, doi:10.1029/2008JD009976, 2008.

Petit, R. H., Legrand, M., Jankowiak, I., Molinié, J., Asselin de Beauville, C., Marion, G., and Mansot, J.-L.: Transport of Saharan dust over the Caribbean Islands: study of an event, J. Geophys. Res., 110, D18S09, doi:10.1029/2004JD004748, 2005.

Prospero, J.: Eolian transport to the world ocean, in: The Sea, edited by: Emiliani, C., Wiley Interscience, NY, 7, 801–874, 1981.

Prospero, J. and Nees, R.: Impact of the North African drought and El Niño on mineral dust in the Barbados trade winds, Nature, 320, 735–738, 1986.

Prospero, J. M. and Carlson, T. N.: Vertical and areal distribution of Saharan dust over the western equatorial north Atlantic Ocean, J. Geophys. Res., 77, 5255–5265, 1972.

Rajot, J.-L., Formenti, P., Alfaro, S. C., et al.: AMMA dust experiment: An overview of measurements performed during the dry season special observation period (SOP0) at the Banizoumbou (Niger) supersite, J. Geophys. Res., 113, doi:10.1029/2008JD009906, D00C14, 2008.

Redelsperger, J.-L., Thorncroft, C., Diedhiou, A., Lebel, T., Parker, D., and Polcher, J.: African monsoon multidisciplinary analysis: An international research project and field campaign , B. Am. Meteorol. Soc., 87, 1739–1746, 2006.

Schepanski, K., Tegen, I., and Macke, A.: Saharan dust transport and deposition towards the tropical northern Atlantic, Atmos. Chem. Phys., 9, 1173–1189, 2009, http://www.atmos-chem-phys.net/9/1173/2009/.

Schladitz, A., Müller, T., Kaaden, N., Massling, A., Kandler, K., Ebert, M., Weinbruch, S., Deutscher, C., and Wiedensohler, A.: In situ measurements of optical properties at Tinfou (Morocco) during the Saharan Mineral Dust Experiment SAMUM 2006, Tellus B, 61, 64–78, 2009.

Seinfeld, J. and Pandis, S.: From Air Pollution to Climate Change, Atmospheric Chemistry and Physics, John Wiley, New York, 1998.

Slingo, T., Ackerman, T., Allan, R., Kassianov, E., McFarlane, S., Barnard, J., Miller, H., Harries, J., Russel, J., and DeWitte, S.: Observation of the impact of a major Saharan dust storm on the atmospheric radiation balance, Geophys. Res. Lett., 33, L24817, doi:10.1029/2006GL027869, 2006.

Tanré, D., Haywood, J., Pelon, J., Léon, J.-F., Chatenet, B., Formenti, P., Francis, P., Goloub, P., Highwood, E., and Myhre, G.: Measurement and modeling of the Saharan dust radiative impact: Overview of the Saharan Dust Experiment (SHADE), J. Geophys. Res., 108(D18), 8574, doi:10.1029/2002JD003273, 2003.

Tesche, M., Ansmann, A., Müller, D., Althausen, D., Engelmann, R., Freudenthaler, V., and Groß, S.: Vertically resolved separation of dust and smoke over Cape Verde using multiwavelength Raman and polarization lidars during Saharan Mineral Dust Experiment 2008, J. Geophys. Res, 114, D13202, doi:10.1029/2009JD011862, 2009.

Tulet, P., Mallet, M., Pont, V., Pelon, J., and Boone, A.: The 7–13 March 2006 dust storm over West Africa: Generation, transport, and vertical stratification, J. Geophys. Res., 113, D00C08, doi:10.1029/2008JD009871, 2008.

Turner, D., Ferrare, R., and Brasseur, L.: Average aerosol extinction and water vapor profiles over the southern great plains, Geophys. Res. Lett., 28, 4441–4444, 2001.